Rapid Communication

Multiband orange–red photoluminescence of Eu^{3+} ions in new "114" $LnBaZn_3GaO_7$ and $LnBaZn_3AlO_7$ oxides

M.P. Saradhi [a,b,c], B. Raveau [c], V. Caignaert [c], U.V. Varadaraju [a,*]

[a] Department of Chemistry, Indian Institute of Technology Madras, Chennai 600 036, India
[b] Department of Chemistry, Indian Institute of Technology Hyderabad, Yeddumailaram, Hyderabad 502205, India
[c] Laboratoire de Cristallographie et Sciences des Matériaux, ENSICAEN, Université de Caen, CNRS, 6 Bd Maréchal Juin, F-14050 Caen 4, France

ARTICLE INFO

ABSTRACT

A new series of gallozincates $LnBaZn_3GaO_7$ (Ln=La, Nd, Sm, Eu, Gd, Dy, Y) and new aluminozincates $LnBaZn_3AlO_7$ (Ln=Y, Eu, Dy) have been synthesized. Their structure refinements show that these phases belong to the "114" series, with hexagonal $P6_3mc$ space group previously described for $SmBaZn_3AlO_7$. The photoluminescence study of these oxides shows that the Eu^{3+} activated $LnBaZn_3MO_7$ oxides with Ln=Y, La, Gd; and M=Al, Ga exhibit strong magnetic and electric dipole transitions (multiband emission) which is of interest for white light production. These results also confirm that the site occupied by Eu^{3+} is not strictly centrosymmetric. The electric dipole transition intensity is the highest in $GdBaZn_3MO_7$ [M=Al, Ga]: 0.05Eu^{3+} as compared with other Eu^{3+} activated compositions. This is due to the layer distortion around GdO_6 octahedra when compared with YO_6 and LaO_6 octahedra.

© 2009 Elsevier Inc. All rights reserved.

1. Introduction

Photoluminescence (PL) of rare-earth ions in different host matrices has been extensively studied for several years by many researchers. Among all the rare-earth ions, the red emitting trivalent Eu^{3+} doped phosphors have significant importance because of their potential application in color display and lighting technologies. In addition, the PL of Eu^{3+} ion is particularly interesting because Eu^{3+} has relatively simple electronic energy level scheme [1] and it acts as a structural probe due to its hypersensitive electronic transitions ($^5D_0 \rightarrow {}^7F_{J=0,1,2}$). From the PL emission spectra, it is possible to understand the number of cationic sites that are available for Eu^{3+} and the symmetry of the site occupied by Eu^{3+}. The presence of multiple cationic sites is clearly indicated by non-degenerate $^5D_0 \rightarrow {}^7F_0$ electronic transition. The forced electric dipole transition $^5D_0 \rightarrow {}^7F_2$ (emission in red region) occurs when Eu^{3+} occupies a site without inversion symmetry [1,2]. This intense single component red emission (around 615 nm) is useful for many practical applications viz., as a red component in tricolor fluorescent lamps (Y_2O_3:Eu^{3+}) [3], cathode ray tubes, electroluminescent devices, field-emission displays [4–7] and for the fabrication of red light emitting diodes (Y_2O_2S:Eu^{3+}; SrY_2S_4:Eu^{2+}) [8,9]. All the applications of Eu^{3+} activated phosphors need not require a single component red

emission ($^5D_0 \rightarrow {}^7F_2$), certain applications prefer multiband emission (orange, $^5D_0 \rightarrow {}^7F_1$; red, $^5D_0 \rightarrow {}^7F_2$). For example, the red emission of Eu^{3+} is a component of artificial white light. If the spectral features of the generated white light need to be similar to that of natural white light, the multiband Eu^{3+} emissions are expected to be quite useful because of the better spectral overlap [10].

Search for stable, novel phosphors with multiband emission properties is therefore, one of the most important aspects in designing luminescent devices. In this respect, aluminates and gallates are potential materials for generating photoluminescence properties, since the band gap of their host lattice is sufficiently large to enable significant emission, when they are doped with Eu^{3+}/Eu^{2+} species. This is the case for instance of $SrAl_2O_4$:Eu^{2+} and similar aluminates with tridymite related structures [11] whose band gap values are around 6 eV. Lantanide aluminates and gallates also represent potential matrices, allowing doping with Eu^{3+}. In fact their number is quite limited, if one excepts $LnAlO_3$:Eu^{3+} [Ln=La, Gd], which exhibits a band gap close to 5.6 eV [12,13]. Some years ago, a series of aluminozincates with the generic formula $LnBaZn_3AlO_7$ (Ln=La, Nd, Sm, Gd, Lu) were synthesized [14,15], which curiously have not been investigated. In the present study, we report on the photoluminescence properties of these aluminozincates and the synthesis, structural characterization and photoluminescence of a new series of isotypic gallozincates $LnBaZn_3GaO_7$ with Ln=Y, La, Sm, Eu, Gd, Dy. We show that for these oxides the band gap values are significantly smaller than for other aluminates, typically

* Corresponding author. Fax: +91 44 22574202.
   E-mail address: varada@iitm.ac.in (U.V. Varadaraju).

~3.9–4.7 eV, but that their electric and magnetic dipole transitions are equally intense, making them promising for the generation of white light.

2. Experimental

2.1. Synthesis

Pechini polymeric sol–gel method was adopted for the synthesis of aluminozincate and gallozincate phases. Pechini method is a useful technique for the preparation of finely divided mixed oxides. This method involves the ability of certain weak alpha-hydroxycarboxylic acids (citric acid) to form polybasic acid chelates with various cations [16,17]. These chelates can undergo polyesterification when heated in a polyhydroxyl alcohol to form a polymeric precursor which has the cations uniformly distributed throughout. The disadvantage of conventional synthesis technique is the necessity of repeated heating and grinding of reactants at various temperatures viz., 400 and 1500 °C for several hours [14,15]. This leads to loss of zinc oxide at higher temperatures and formation of non-stoichiometric/multiphase compounds. Pechini method avoids the difficulties associated for the synthesis of these phases by solid state method. A flow chart for the synthesis of $LnBaZn_3MO_7$ [Ln=Y, La, Nd, Sm, Eu, Gd, Dy; M=Al, Ga] phases is given in Fig. 1. Required amounts of metal nitrates (M) and citric acid (CA) in the molar ratio of 1:3 (M to CA=1:3) were dissolved in distilled H_2O and stirred at 60 °C/6 h until a clear solution is obtained. To this metal citrate complex solution, ethylene glycol (EG) was added in 1:3 molar ratio (CA:EG-1:3) and stirred at 90 °C/6 h. The obtained viscous solution was further heated at 140 °C to distil off excess EG and to induce esterification. This resulted in a substantial increase in solution viscosity. The dense viscous solution was vacuum dried at 180 °C to yield organic polymer foam. The obtained polymer foam was subsequently decomposed at 300 °C/6 h. The final heat treatment for these compounds was done at 1000 °C/12 h.

2.2. Characterization

Thermogravimetric (TG) analysis of the prepared polymeric precursors was performed in air with a heating rate of 5 °C/min using a Perkin Elmer thermobalance. Fig. 2 shows as an example the TG/DTG curves of the precursor that was obtained after decomposing the polymeric gel at 300 °C for 3 h for $EuBaZn_3GaO_7$. The slope region from RT to 350 °C is due to the dehydration of precursor (water loss) with a weight loss of 7%. The larger mass loss between temperature intervals of 400 to 500 °C is attributed to the pyrolysis of the citrate and ethylene glycol, resulting from the decomposition of organic constituents and the release of NO_x and CO_x gases from the polymer precursor [18]. All the compositions were checked for phase formation by recording powder X-ray diffraction (XRD) using Panalytical X'pert diffractometer equipped with $CuK\alpha_1$ radiation. The sample morphology was studied with a scanning electron microscope (SEM) Philips Field Effect Gun (FEG) XL-30 with a resolution of about 1 nm. Fig. 3 shows as example SEM micrographs of the phase $EuBaZn_3GaO_7$ calcined at 1000 °C/12 h. The morphology of the as synthesized sample shows agglomerated particles with average diameter of about 1 μm. Diffuse reflectance spectra (DRS) of the samples were recorded using an UV–visible spectrophotometer with integrating sphere attachment (Jasco, V550). $BaSO_4$ was used as the reference. PL excitation and emission spectra at RT was recorded on powder samples using a
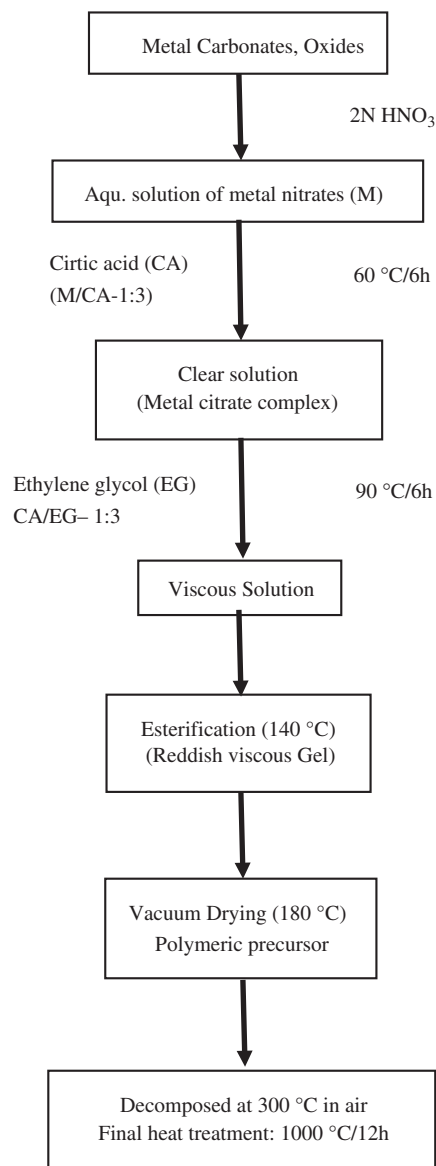

Fig. 1. Flow chart of the synthesis procedure for the compositions $LnBaZn_3MO_7$ [M=Al, Ga].
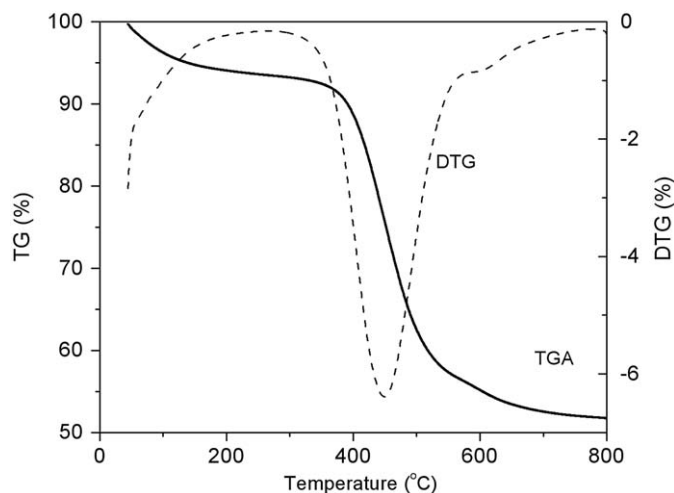

Fig. 2. TGA and DTG curves of polymeric precursor $EuBaZn_3GaO_7$ calcined at 300 °C.
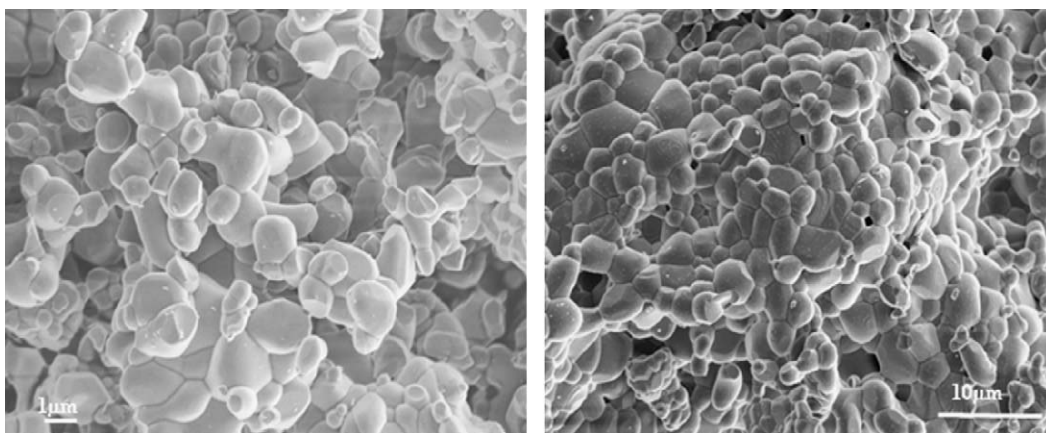
Fig. 3. SEM micrographs of as synthesized EuBaZn₃GaO₇.

Horiba Jobin Yvon Fluorolog-3 spectrofluorometer having 450 W xenon lamp with operating range 220–850 nm.

3. Results and discussions

3.1. Synthesis and structural characterization

Using the Pechini polymeric sol–gel method, described above, we have synthesized seven new gallozincates $LnBaZn_3GaO_7$ with Ln=La, Nd, Sm, Eu, Gd, Dy, Y and three new aluminozincates $LnBaZn_3AlO_7$ with Ln=Eu, Dy, Y. The X-ray powder diffraction patterns of all these oxides show that they are all isotypic to the $LnBaZn_3AlO_7$ compounds, with Ln=La, Nd, Sm, Gd, Lu previously synthesized by Müller-Buschbaum and Rabbow. Hence, the starting structure model for structure refinement is taken as the one reported earlier [14,15]. Structure refinements were carried out in the space group $P6_3mc$, by Rietveld method using FULLPROF program [19]. All the Rietveld refinements were done in the same way as described below. The background was selected manually; pseudo-voigt function was used to model the peak shape. After the successful refinement of instrumental zero shift, scale factor and peak shape, the distribution of Zn/Ga atoms between two crystallographic sites $2a$ and $6c$ was refined by assigning constraints. Finally, the asymmetric parameters, atomic positions and isothermal parameters were refined. The observed, calculated and difference patterns of EuBaZn₃GaO₇ phases are shown in Fig. 4. The obtained profile factors of all the phases $LnBaZn_3GaO_7$ [Ln=Y, La, Nd, Sm, Eu, Gd, Dy] reveal that the fitting quality is good. The refined lattice parameters, atomic coordinates and obtained Bragg R and R_f factors are given in Table 1. The structure consists of two types of corner sharing Zn/AlO₄ tetrahedra located in separate alternate stacked layers of triangular ($2a$ site) and Kagomé ($6c$) type with statistical distribution of Zn and Al atoms between the two tetrahedral sites. Ba²⁺ cations are present in 12 coordinated anticuboctahedron site with respect to the oxygens. The Ln^{3+} cations exhibit an octahedral coordination with 3-fold rotational symmetry [14,15,20,21]. The variation in both of 'a' and 'c' lattice parameters with increasing size of the rare earths is nonlinear. This may be due to the difference in the distribution of 'Zn' between $2a$ and $6c$ lattice sites. It is known that as the ionic radius of the rare earth ion increases Zn²⁺ preferably occupies the $6c$ site [20,21]. The obtained bond lengths from structure refinement data of both aluminates and gallates are given in Tables 2 and 3.
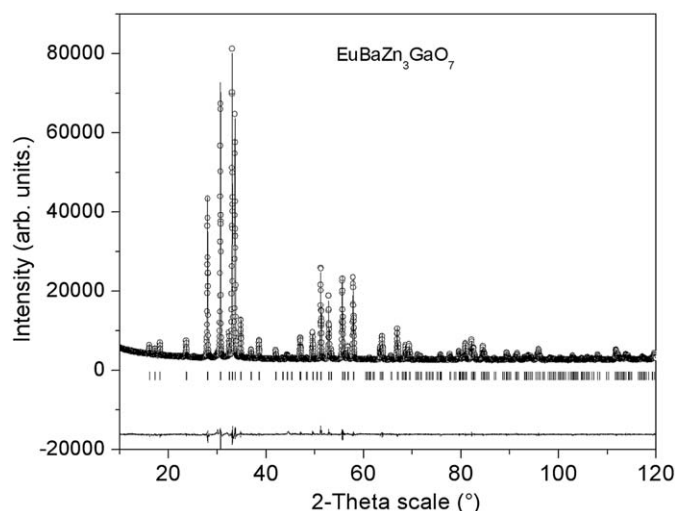

Fig. 4. Observed, calculated and difference powder X-ray diffraction profiles of EuBaZn₃GaO₇.

3.2. Diffuse reflectance spectroscopy

The diffuse reflectance spectra of gallozincates $LnBaZn_3GaO_7$ are shown in Fig. 5. The optical band gap values were calculated from the absorption edge using Kubelka–Munk function which is given by $(K–M)=(1–R)^2/2R$, where R is the reflectance value. The value of the wavelength is substituted in the formula E (eV)=1236/wavelength (nm). Strong absorption band at around 270 to 320 nm is observed for all the compositions, which is attributed to the host absorption. The obtained band gap values for the various gallate and aluminate phases are listed in Table 4. A decrease in the optical band gap is observed by changing the rare earth ion from smaller Y to bigger La. This can be due to the decrease in the polarizability of the anion, O^{2-} with increasing size of counter cation (rare earth) resulting in the observed decrease in optical band gap. In EuBaZn₃GaO₇, Eu³⁺ absorption bands are observed from $^7F_0$ to $^5d_{(=1, 2 \text{ and } 4)}$ electronic levels at 362, 395 ($^5L_6$), 465 and 556 nm [22]. SmBaZn₃GaO₇ shows weak absorption bands at around 377, 404, 466 nm which are due to the electronic transition of $^6H_{5/2} \rightarrow {}^4K_{j(=11/2, 13/2 \text{ and } 17/2)}$ of Sm³⁺ [22]. In the case of NdBaZn₃GaO₇, the various absorption bands observed in the visible and near IR region are due to Nd³⁺. The bands are assigned to excitation from the ground state $^4I_{9/2}$ to various excited states $^4F_{j(=5/2 \text{ and } 7/2)}$ and $^4G_{j(=5/2 \text{ and } 7/2)}$ of Nd³⁺ [22].

Table 1
Atomic coordinates and agreement factor of LnBaZn$_3$GaO$_7$.

	YBaZn$_3$GaO$_7$	LaBaZn$_3$GaO$_7$	NdBaZn$_3$GaO$_7$	SmBaZn$_3$GaO$_7$
2b	Y 2/3,1/3,0.819(1)	La 2/3,1/3,0.812(3)	Nd 2/3,1/3,0.847(6)	Sm 2/3,1/3,0.815(4)
2b	Ba 2/3, 1/3, 0.445(3)	Ba 2/3,1/3,0.440(3)	Ba 2/3,1/3,0.474(6)	Ba 2/3,1/3,0.443(3)
6c	Zn, Ga—(0.94(5),0.05(8))[a] 0.170(8),0.829(5),0.630(7)	Zn, Ga—(0.92(5), 0.05(5))[a] 0.169,0.830,0.623(2)	Zn, Ga—(0.87(9), 0.12)[a] 0.153(1),0.846(8),0.467(4)	Zn, Ga—(0.78(5),0.22(5))[a] 0.169(5),0.830(4),0.629
2a	Zn, Ga—(0.17(2),0.82(4))[a] 0.0,0.0,0.883	Zn, Ga—(0.23(1), 0.77(6))[a] 0.0,0.0,0.885(1)	Zn Ga—(0.36, 0.63(9))[a] 0.0,0.0,0.913(6)	Zn, Ga—(0.66(1),0.34(1))[a] 0.0,0.0,0.880(4)
6c	O 0.166(4),0.833(6),0.444(5)	O 0.159(5),0.840,0.436	O 0.153(1),0.846(7),0.467(4)	O 0.163(3),0.836(3),0.438
6c	O 0.501(6),0.498(3),0.696(5)	O 0.495(2),0.504(1),0.680(4)	O 0.495(2),0.505(4),0.680(4)	O 0.493(1),0.506(1),0.687
2a	O 0.0,0.0,0.702	O 0.0,0.0,0.692(6)	O 0.0, 0.0, 0.707	O 0.0,0.0,0.688(2)
a (Å)	6.322	6.457(5)	6.369(5)	6.381(6)
c (Å)	10.273	10.346(1)	10.251(6)	10.306(6)
R$_{wp}$	5.04	6.40	4.35	4.35
Bragg R-factor	3.0	5.6	3.6	3.6
R$_f$	4.0	5.1	3.14	3.14
χ^2	8.88	8.90	3.88	3.88

	EuBaZn$_3$GaO$_7$	GdBaZn$_3$GaO$_7$	DyBaZn$_3$GaO$_7$
2b	Eu 2/3,1/3,0.825(3)	Gd 2/3,1/3,0.819(3)	Dy 2/3,1/3,0.822(1)
2b	Ba 2/3, 1/3, 0.452(1)	Ba 2/3,1/3,0.446(4)	Ba 2/3,1/3,0.449(2)
6c	Zn, Ga—(0.72(5),0.28(5))[a] 0.169(8),0.830(2),0.638(1)	Zn, Ga—(0.93,0.07(5))[a] 0.170(2),0.829(8),0.629(3)	Zn, Ga—(0.83(4),0.17)[a] 0.169(8),0.830(1),0.635(2)
2a	Zn, Ga—(0.84(4),0.16(4))[a] 0.0,0.0,0.885(5)	Zn, Ga—(0.20,0.80(4))[a] 0.0,0.0,0.889(4)	Zn Ga—(0.52,0.48(3))[a] 0.0,0.0,0.887(3)
6c	O 0.160(1),0.839(1),0.446(9)	O 0.166(5),0.833(5),0.443(4)	O 0.165(2),0.834(7),0.448(1)
6c	O 0.494(2),0.394(2),0.692(7)	O 0.492,0.507(9),0.688(8)	O 0.492(4),0.507(6),0.692(7)
2a	O 0.0,0.0,0.696(4)	O 0.0,0.0,0.691(2)	O 0.0, 0.0, 0.696
a (Å)	6.368(2)	6.359(3)	6.367(2)
c (Å)	10.303(1)	10.299(9)	10.307(6)
R$_{wp}$	3.5	3.28	3.57
Bragg R-factor	5.19	5.98	4.78
R$_f$	4.78	7.32	5.57
χ^2	4.54	5.69	4.90

[a] Occupancy of Zn and Ga in 6c and 2a sites.

Table 2
Selected interatomic distances (Å) for LnBaZn$_3$AlO$_7$ [Ln=Y, La, Nd, Sm, Eu, Gd, Eu, Dy].

Y–O(1) × 3	2.25(1)	Ba–O(1) × 6	3.14(9)
–O(2) × 3	2.20(1)	–O(2) × 3	3.04(1)
		–O(2) × 3	3.22(1)
Zn(1)/Al(1)–O(1)	1.93(2)	Zn(2)/Al(2)–O(1) × 3	1.85(1)
Zn(1)/Al(1)–O(2) × 2	1.91(4)	Zn(2)/Al(2)–O(3)	1.91(1)
Zn(1)/Al(1)–O(3)	1.96(1)		
La–O(1) × 3	2.35(2)	Ba–O(1) × 6	3.21(1)
–O(2) × 3	2.36(2)	–O(2) × 3	3.09(1)
		–O(2) × 3	3.24(2)
Zn(1)/Al(1)–O(1)	1.97(2)	Zn(2)/Al(2)–O(1) × 3	1.83(2)
Zn(1)/Al(1)–O(2) × 2	1.89(2)	Zn(2)/Al(2)–O(3)	1.78(1)
Zn(1)/Al(1)–O(3)	1.98(4)		
Nd–O(1) × 3	2.33(2)	Ba–O(1) × 6	3.18(3)
–O(2) × 3	2.34(3)	–O(2) × 3	3.09(2)
		–O(2) × 3	3.21(4)
Zn(1)/Al(1)–O(1)	1.95(3)	Zn(2)/Al(2)–O(1) × 3	1.77(1)
Zn(1)/Al(1)–O(2) × 2	1.88(1)	Zn(2)/Al(2)–O(3)	1.91(4)
Zn(1)/Al(1)–O(3)	1.98(2)		
Sm–O(1) × 3	2.30(1)	Ba–O(1) × 6	3.17(8)
–O(2) × 3	2.33(1)	–O(2) × 3	3.11(4)
		–O(2) × 3	3.19(3)
Zn(1)/Al(1)–O(1)	1.89(1)	Zn(2)/Al(2)–O(1) × 3	1.83(1)
Zn(1)/Al(1)–O(2) × 2	1.88(1)	Zn(2)/Al(2)–O(3)	1.95
Zn(1)/Al(1)–O(3)	1.99(2)		
Eu–O(1) × 3	2.25(1)	Ba–O(1) × 6	3.16(6)
–O(2) × 3	2.39(1)	–O(2) × 3	3.10(4)
		–O(2) × 3	3.19(8)
Zn(1)/Al(1)–O(1)	1.89(1)	Zn(2)/Al(2)–O(1) × 3	1.90(2)

Table 2. (continued)

Zn(1)/Al(1)–O(2) × 2	1.84(1)	Zn(2)/Al(2)–O(3)	1.95(0)
Zn(1)/Al(1)–O(3)	1.96(4)		
Gd–O(1) × 3	2.23(4)	Ba–O(1) × 6	3.16(5)
–O(2) × 3	2.38(3)	–O(2) × 3	3.05(3)
		–O(2) × 3	3.23(2)
Zn(1)/Al(1)–O(1)	1.90(9)	Zn(2)/Al(2)–O(1) × 3	1.89(4)
Zn(1)/Al(1)–O(2) × 2	1.84(4)	Zn(2)/Al(2)–O(3)	1.91(1)
Zn(1)/Al(1)–O(3)	1.98(4)		
Dy–O(1) × 3	2.21(2)	Ba–O(1) × 6	3.14(1)
–O(2) × 3	2.35(6)	–O(2) × 3	3.04(4)
		–O(2) × 3	3.23(4)
Zn(1)/Al(1)–O(1)	1.88(0)	Zn(2)/Al(2)–O(1) × 3	1.96(0)
Zn(1)/Al(1)–O(2) × 2	1.84(3)	Zn(2)/Al(2)–O(3)	1.78(0)
Zn(1)/Al(1)–O(3)	2.01(0)		

### 3.3. Photoluminescence spectroscopy

The photoluminescence excitation and emission spectra of EuBaZn$_3$MO$_7$ [M=Ga, Al] are shown in Fig. 6. The excitation spectra of both gallium and aluminum zincates show a broad band at around 280 nm, which is due to the $^7F_0$ ground state to the charge transfer states (CTS) caused by the transfer of electron from oxygen 2p orbital to the empty 4f orbital of Eu^{3+} [Fig. 6(a)]. In addition, there are several sharp lines observed, which are due to the intra-4f transitions [1]. The intensity of the Eu^{3+}–O^{2-} CT band in the aluminate is comparable to that of the sharp intra

Table 3
Selected interatomic distances (Å) for LnBaZn$_3$GaO$_7$ [Ln=Y, La, Nd, Sm, Eu, Gd, Dy].

Y–O(1) × 3	2.20(4)	Ba–O(1) × 6	3.16(1)
–O(2) × 3	2.22(3)	–O(2) × 3	3.04(3)
		–O(2) × 3	3.25(2)
Zn(1)/Ga(1)–O(1)	1.95(4)	Zn(2)/Ga(2)–O(1) × 3	1.91(1)
Zn(1)/Ga(1)–O(2) × 2	1.92(1)	Zn(2)/Ga(2)–O(3)	1.91(7)
Zn(1)/Ga(1)–O(3)	1.98(2)		
La–O(1) × 3	2.32(7)	Ba–O(1) × 6	3.22(9)
–O(2) × 3	2.35(6)	–O(2) × 3	3.13(4)
		–O(2) × 3	3.24(3)
Zn(1)/Ga(1)–O(1)	1.94(2)	Zn(2)/Ga(2)–O(1) × 3	1.86(3)
Zn(1)/Ga(1)–O(2) × 2	1.91(1)	Zn(2)/Ga(2)–O(3)	1.99(0)
Zn(1)/Ga(1)–O(3)	2.02(4)		
Nd–O(1) × 3	2.30(2)	Ba–O(1) × 6	3.20(5)
–O(2) × 3	2.32(1)	–O(2) × 3	3.10(4)
		–O(2) × 3	3.21(2)
Zn(1)/Ga(1)–O(1)	1.92(3)	Zn(2)/Ga(2)–O(1) × 3	1.85(1)
Zn(1)/Ga(1)–O(2) × 2	1.88(1)	Zn(2)/Ga(2)–O(3)	1.95(4)
Zn(1)/Ga(1)–O(3)	1.98(2)		
Sm–O(1) × 3	2.26(4)	Ba–O(1) × 6	3.19(1)
–O(2) × 3	2.32(3)	–O(2) × 3	3.15(4)
		–O(2) × 3	3.17(4)
Zn(1)/Ga(1)–O(1)	1.96(1)	Zn(2)/Ga(2)–O(1) × 3	1.90(3)
Zn(1)/Ga(1)–O(2) × 2	1.88(1)	Zn(2)/Ga(2)–O(3)	1.98
Zn(1)/Ga(1)–O(3)	1.96(3)		
Eu–O(1) × 3	2.28(2)	Ba–O(1) × 6	3.18(1)
–O(2) × 3	2.34(2)	–O(2) × 3	3.12(4)
		–O(2) × 3	3.20(8)
Zn(1)/Ga(1)–O(1)	1.97(1)	Zn(2)/Ga(2)–O(1) × 3	1.87(3)
Zn(1)/Ga(1)–O(2) × 2	1.87(1)	Zn(2)/Ga(2)–O(3)	1.94(0)
Zn(1)/Ga(1)–O(3)	1.96(4)		
Gd–O(1) × 3	2.23(4)	Ba–O(1) × 6	3.18(0)
–O(2) × 3	2.34(6)	–O(2) × 3	3.15(4)
		–O(2) × 3	3.17(6)
Zn(1)/Ga(1)–O(1)	1.92(0)	Zn(2)/Ga(2)–O(1) × 3	1.92(2)
Zn(1)/Ga(1)–O(2) × 2	1.87(1)	Zn(2)/Ga(2)–O(3)	1.97(0)
Zn(1)/Ga(1)–O(3)	1.97(3)		
Dy–O(1) × 3	2.26(3)	Ba–O(1) × 6	3.18(4)
–O(2) × 3	2.33(9)	–O(2) × 3	3.16(1)
		–O(2) × 3	3.17(6)
Zn(1)/Ga(1)–O(1)	1.92(0)	Zn(2)/Ga(2)–O(1) × 3	1.92(2)
Zn(1)/Ga(1)–O(2) × 2	1.87(1)	Zn(2)/Ga(2)–O(3)	1.97(0)
Zn(1)/Ga(1)–O(3)	1.97(0)		

Table 4
Optical band gap values of LnBaZn$_3$MO$_7$ [M=Al, Ga].

Compound	Optical band gap (eV)	Compound	Optical band gap (eV)
YBaZn$_3$GaO$_7$	4.38	YBaZn$_3$AlO$_7$	4.70
LaBaZn$_3$GaO$_7$	4.00	LaBaZn$_3$AlO$_7$	4.59
NdBaZn$_3$GaO$_7$	3.98	NdBaZn$_3$AlO$_7$	4.28
SmBaZn$_3$GaO$_7$	4.16	SmBaZn$_3$AlO$_7$	4.52
EuBaZn$_3$GaO$_7$	4.24	EuBaZn$_3$AlO$_7$	4.65
GdBaZn$_3$GaO$_7$	4.26	GdBaZn$_3$AlO$_7$	4.67
DyBaZn$_3$GaO$_7$	4.30	DyBaZn$_3$AlO$_7$	4.69
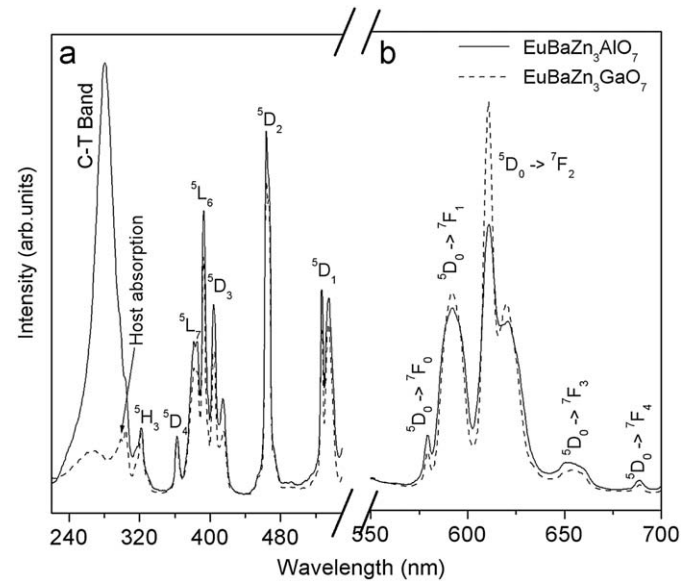
Fig. 6. PL excitation (a) and emission (b) spectra of EuBaZn$_3$MO$_7$ [M=Al, Ga] −0.05Eu^{3+} under 465 nm excitation wavelength.
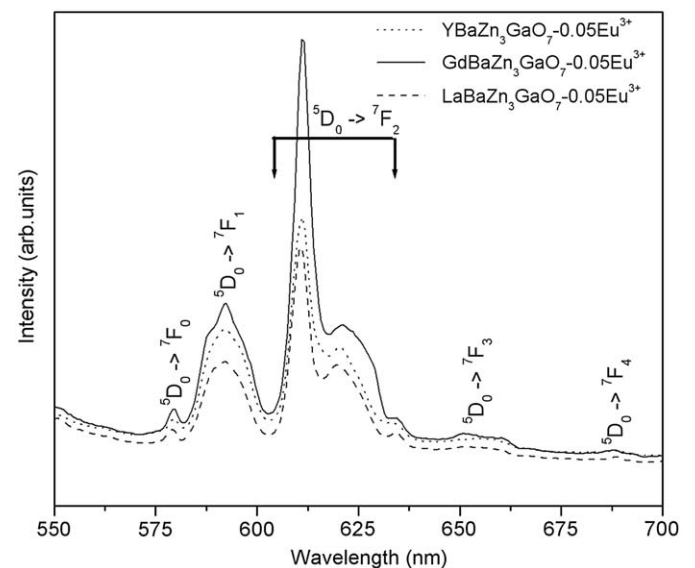
Fig. 7. PL emission spectra of LnBaZn$_3$GdO$_7$ [Ln=Y, La and Gd] −0.05Eu^{3+} under λ_{ex}=465 nm excitation wavelength.

Fig. 5. UV–vis diffuse reflectance spectra of LnBaZn$_3$GaO$_7$ [Ln=Y, La, Nd, Sm, Eu Gd and Dy].

$4f$–$4f$ Eu^{3+} lines. The emission spectra of both the Eu^{3+} activated gallate and aluminate show multi-band emission, which is a useful component for white light generation. The emission spectra consist of intense lines at around 615 nm (red) and
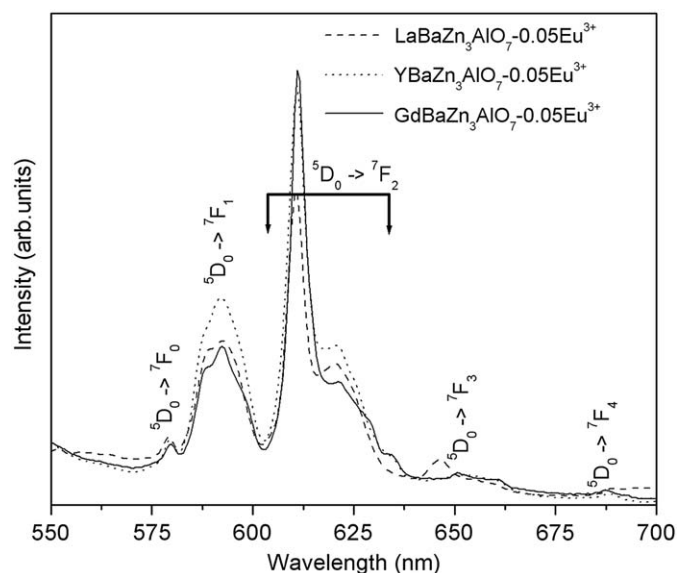
Fig. 8. PL emission spectra of LnBaZn$_3$AlO$_7$ [Ln=Y, La and Gd] $-$0.05Eu^{3+} under λ_{ex}=465 nm excitation wavelength.

591 nm (orange–red) corresponding to $^5D_0 \rightarrow {^7F_2}$ electric dipole (ED) and magnetic dipole (MD) transitions, respectively. The presence of unique emission line at 576 nm ($^5D_0 \rightarrow {^7F_0}$) indicates that Eu^{3+} occupies only one site in the lattice. The presence of both ED and MD electronic transitions in the emission spectra confirms that the site occupied by Eu^{3+} in this host lattice is not strictly centrosymmetric. The observed weak emission bands at 650 and 688 nm are due to the $^5D_0 \rightarrow {^7F_{j(=3,4)}}$ electronic transitions. Figs. 7 and 8 show the emission spectra of other rare earth gallium and aluminum zincates LnBaZn$_3$MO$_7$ [Ln=Y,La Gd; M=Al, Ga] activated with 5 mole% of Eu^{3+}. The emission spectra of both gallates and aluminates exhibit same spectral features when compared with the EuBaZn$_3$MO$_7$ [M=Ga, Al]. The band corresponding to the ED transition is highest in intensity in GdBaZn$_3$MO$_7$ [M=Al, Ga]:0.05Eu^{3+} when compared with the other Eu^{3+} activated compositions. This is in very good agreement with structural data. From Tables 2 and 3, it is clear that the GdO$_6$ octahedra are more distorted than the LaO$_6$ or YO$_6$ octahedra. The larger degree of distortion in the local symmetry of Eu^{3+} ions leads to an enhancement of the $^5D_0 \rightarrow {^7F_2}$, ED transitions [23].

4. Concluding remarks

New gallozincates and aluminozincates, LnBaZn$_3$MO$_7$ (M=Ga, Al) with Ln=La, Nd, Sm, Eu, Gd, Dy, Y and Ln=Eu, Dy, Y,

respectively, have been synthesized and shown to belong to "114" structural series previously isolated by Rabbow and Müller-Buschbaum [13,14], consisting of the stacking of kagomé and triangular layers of GaO$_4$(AlO$_4$) and ZnO$_4$ tetrahedra forming octahedral cavities occupied by lanthanide cations. Their UV–vis diffuse reflectance spectra show that the matrix of these oxides exhibits smaller band gaps of $\sim$3.9–4.7 eV, compared to pure aluminates ($\sim$6 eV), probably due to the presence of a majority of zinc in the structure. It is also observed that the band gap of these oxides is larger for smaller lanthanides (Y, Dy) than for the larger ones (La, Nd) in agreement with the fact that the Y/Dy–O bond is less ionic and consequently that the Zn/(Al/Ga)–O bond in the former oxides becomes less covalent. More importantly, it is demonstrated that these compounds exhibit multiband photo-luminescence emission in orange and red region, which is useful for generating white light. Moreover, it is remarkable that the emission intensity of ED transition of GdBaZn$_3$MO$_7$ [M=Al, Ga]:0.05Eu^{3+} is higher when compared with other rare earth containing compositions LnBaZn$_3$MO$_7$ [Ln=Y, La; M=Al, Ga]. This is in line with the structural data. The GdO$_6$ octahedra are more distorted than the LaO$_6$ or YO$_6$ octahedra.

References

[1] G. Blasse, B.C. Grabmaier, Luminescent Materials, Springer, Berlin, 1994.
[2] R. Jagannathan, M. Kottaisamy, J. Phys. Condens. Matter 7 (1995) 8453–8466.
[3] Y. Jüstel, N. Hans, R. Cees, Angew. Chem. Int. Ed. 37 (1998) 3084–3103.
[4] W. Xu, W. Jia, I. Revira, K. Monge, H. Liu, J. Electrochem. Soc. 148 (2001) H176–H178.
[5] S.-J. Park, C.-H. Park, B.-Y. Yu, H.-S. Base, C.-H. Kim, C.-H. Pyun, J. Electrochem. Soc. 146 (1999) 3903–3906.
[6] C.R. Ronda, T. Justel, H. Nikol, J. Alloys Compd. 275–277 (1998) 669–676.
[7] R. Reisfeld, C.K. Jorgensen, Lasers and Excited States of Rare Earths, Springer, New York, 1997.
[8] T. Nishida, T. Ban, N. Kobayashi, Appl. Phys. Lett. 82 (2003) 3817–3819.
[9] Y. Huh, J. Park, S. Kweon, Ji. Kim, J. Kim, Y. Rag Do, Bull. Korean Chem. Soc. 25 (2004) 1585–1588.
[10] Shinobu Fujihara, Kazuaki Tokumo, Chem. Mater. 17 (2005) 5587–5593.
[11] S.H.M. Poort, W.P. Blokpoel, G. Blasse, Chem. Mater. 7 (1995) 1547–1551.
[12] Z. Zhong, P.J. Kelly, EPL 84 (2008) 27001p4–27001p5.
[13] H.H.S. Oliveira, M.A. Cebim, A.A. Da Silva, M.R. Davolos, J. Alloys Compd. 488 (2009) 619–623.
[14] Ch. Rabbow, Hk. Müller-Buschbaum, Z. Naturforsch. 51b (1996) 343–347.
[15] Ch. Rabbow, Hk. Müller-Buschbaum, Z. Naturforsch. 52b (1997) 546–548.
[16] P. Pechini, Maggio, 1967. US Pat. 3,330,697.
[17] W. Liu, G.C. Farrington, J. Electrochem. Soc. 143 (1996) 879–884.
[18] Ch. Laberty-Robert, F. Ansart, C. Deloget, M. Gaudon, A. Rousset, Mat. Res. Bull. 36 (2001) 2083–2101.
[19] J. Rodríguez-Carvajal, An Introduction to the Program FullProf 2000, Version July 2001.
[20] M. Valldor, Solid State Sci. 6 (2004) 251–266.
[21] M. Valldor, Remnant magnetization above room temperature in the semiconductor Y$_{0.5}$Ca$_{0.5}$BaCo$_4$O$_7$, Solid State Sci. 8 (2006) 1272–1280.
[22] G.H. Dieke, Spectra and Energy Levels of Rare Earth Ions in Crystals, Wiley, New York, 1968.
[23] Yue Zhang, Ya Dong Li, J. Alloys Comp. 370 (2004) 99–103.